Available online at www.sciencedirect.com

ScienceDirect

Scripta Materialia 71 (2014) 9–12

Scripta MATERIALIA

www.elsevier.com/locate/scriptamat

Grain size effects in the deformation of [0001] textured nanocrystalline Zr

C.J. Ruestes,[a] G. Bertolino,[b] M. Ruda,[c,*] D. Farkas[d] and E.M. Bringa[e]

[a]*Instituto Balseiro-Instituto de Ciencias Básicas, Univ. Nac. Cuyo, Argentina*
[b]*CONICET, Centro Atómico Bariloche, 8400 Bariloche, Argentina*
[c]*CNEA-Centro Atómico Bariloche-Univ. Comahue, 8400 Bariloche, Argentina*
[d]*Department of Materials Science and Engineering, Virginia Tech, Blacksburg, VA 24061, USA*
[e]*CONICET-Instituto de Ciencias Básicas, Univ. Nac. Cuyo, Mendoza 5500, Argentina*

Received 3 May 2013; revised 29 August 2013; accepted 8 September 2013
Available online 17 September 2013

Molecular dynamics was used to simulate tensile testing of columnar grain samples of nanocrystalline Zr with random rotations around the [0001] axis. For grain sizes smaller than a critical size the results show an inverse Hall–Petch effect. For larger grains the calculated Hall–Petch constant agrees well with the experimental data. Grain size effects on deformation mechanisms, including grain boundary sliding and dislocation emission, are also discussed.

Keywords: Zirconium; Nanocrystalline materials; Hall–Petch effect; Molecular dynamics (MD)

In the past decades extensive research has been performed on the preparation, characterization and simulation of nanocrystalline (nc) materials, due to their special mechanical properties when compared with conventional polycrystalline materials [1–6]. Most of this work has concentrated on face-centered cubic (fcc) metals.

Zirconium, an hexagonal close-packed (hcp) metal with high resistance to corrosion and irradiation as well as good biocompatibility, has been extensively used in various applications such as the nuclear industry. There is a strong interest in Zr and Zr alloys with a nanoscale microstructure that might offer improved mechanical properties. Experimental mechanical properties of hcp Zr single crystals [7] or polycrystals with grain sizes of a few microns have been available for some time now [8,9]. Going from coarse grains to nanograins has not been an easy task and many different methods have been tried [10–15]. Most of these involve surface modifications such as a combination of extrusion, drawing and annealing [10], surface mechanical attrition treatment [11], surface circulation rolling treatment at cryogenic temperatures [12] or cryorolling annealed Zr at high strain rates [13]. The results generally lead to samples with grain size distributions ranging from the nanoscale to the microscale. Micropillar samples of hcp nc-Zr (grain size ~30 nm) were fabricated from thin films using focussed ion beam machining, and engineering stress–strain curves were obtained under compression, showing plastic behavior up to 12% deformation [14]. Thin films of nc-Zr with columnar grain sizes ranging between 10 and 55 nm were manufactured by Wang et al. [15] using magnetron sputtering. Indentation tests showed an inverse Hall–Petch behavior below a critical grain diameter of ~30 nm.

Molecular dynamics (MD) has been widely used to gain insight into the effects of grain size on the mechanical properties of nanocrystalline metallic systems [16]. Most simulations have focused on fcc metals [17–21] or body-centered cubic (bcc) metals [22], but recently they have been extended to hcp metals such as Mg ($c/a = 1.624$) [23–26] and Ti ($c/a = 1.587$) [26]. In this paper we will address nc-Zr ($c/a = 1.593$).

The samples for the MD simulations reported here were generated using a Voronoi construction with random misorientation angles around the [0001] axis and random grain boundary orientations. This texture is often found in plates or tubes of different Zr alloys used in

* Corresponding author. Tel.: +54 2944445278; fax: +54 2944445299;
e-mail addresses: margaritaruda@yahoo.com; ruda@cab.cnea.gov.ar

1359-6462/$ - see front matter © 2013 Acta Materialia Inc. Published by Elsevier Ltd. All rights reserved.
http://dx.doi.org/10.1016/j.scriptamat.2013.09.010

the nuclear industry [27–30]. The procedure to generate the simulation samples was similar to that used in a previous work on columnar fcc structures [18]. All the grain boundaries (GBs) in the textured sample were of tilt character, with random misorientation angles around the [0001] axis. Figure 1 shows the initial structure of a six-grain sample. It should be pointed out that in this study grain shapes are random, rather than the hexagonal columns used in previous MD studies of hcp materials [23–26]. Periodic boundary conditions were used in all directions, with the periodicity in the [0001] direction being that of the crystalline lattice. The average grain size varied from 7 to 130 nm (10^4–2.3×10^6 atom samples) by changing the simulation domain dimensions while keeping the number and geometry of grains unchanged, obtaining self-similar samples.

Strain-controlled tensile deformation was applied perpendicular to the [0001] axis, keeping zero pressure in the other two directions. In this geometry, only straight dislocations can be observed as a result of the deformation. The geometry was chosen to allow the activation of the $\langle 11\text{–}20\rangle\{1\text{–}100\}$ first-order prismatic slip. We can focus on the interplay between dislocation emission and GB sliding because twinning rarely appears with this orientation [27]. However, we note that the geometry of our samples does not allow the study of all the possible twins that have been observed in Zr which may have important effects in the behavior of nanocrystalline Zr [31–37].

The MD simulations were performed using LAMMPS [38] and the embedded atom method (EAM) potential by Pasianot and Monti [39]. Elastic constants of hcp Zr depicted by EAM potentials are representative of experimental values [40]. In general, the ability of EAM potentials to properly describe slip system choice and dislocation core structure in Zr is more problematic than in fcc metals. Recently, the core structure of screw dislocations was calculated using ab initio and EAM calculations, with encouraging results [41]. The choice of slip system in our simulations is limited by the sample geometry.

The samples were relaxed for 30 ps at 300 K and 0 bar pressure to achieve a relaxed GB structure. After relaxation a uniaxial tensile test was simulated at a constant strain rate and zero pressure in the directions perpendicular to the tensile axis. Two strain rates, 1×10^8 and 5×10^8 s^{-1}, were used, and two different temperatures, 10 and 300 K, controlled by a Nosé–Hoover thermostat. The stress–strain curves obtained are shown in Figure 2a for different grain sizes. The resulting structures and deformation mechanisms were visualized using OVITO [42] and its built-in common neighbor analysis (CNA).

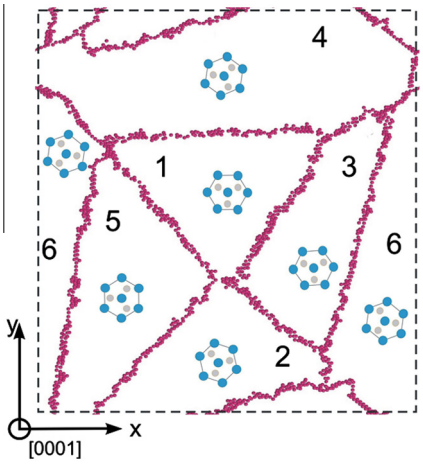

GB	θ [°]
1-2	20
1-3	-5
1-4	23
1-5	31
1-6	37
2-3	25
2-4	3
2-5	11
2-6	17
3-4	28
3-6	42
4-6	14
5-6	6

Figure 1. Sample visualization, showing misorientations of the grains and grain boundaries. Only non-hcp atoms are shown, as filtered by common-neighbor analysis (CNA) [42].

The shape of the stress–strain curves is similar to curves for fcc [17] and bcc [22] nanocrystalline metals, and also similar to recently presented curves for nanocyrstalline Mg [23]. The maximum stresses, in the range 1.6–2 GPa, are much larger than experimental yield stress values for Zr with micron-size grains, in the range ~0.3–0.5 GPa [43], as expected for nanocrystalline samples [1–6]. The oscillations in the stress at large strains are due to the relatively small number of grains included in our sample. To ensure that the average stresses are independent of the number of grains, we carried out some selected simulations doubling the number of grains, and found that oscillations are greatly reduced, but the average flow stress does not change compared to the smaller simulations, within a ~10% error.

The average flow stresses of our nc Zr samples were calculated between 5% and 12% strain and their variation with the inverse square root of the grain size d is displayed in Figure 2b for two different temperatures. Our simulation data also showed that the maximum flow stress decreases with decreasing strain rate, and the effect is more important at large grain sizes. This behavior has been found in many MD studies [21,43–45], which conclude that the lower strain rates allow for more time available for defects to nucleate and accommodate the applied strain, reducing the resulting flow stress.

The average flow stresses in our simulations are lower at higher temperatures, as expected. We found for a sample with average grain size $d \approx 40$ nm ($1/d^{0.5} = 0.16\ \mathrm{nm}^{-0.5}$) a maximum stress and a flow stress that are 28% lower at 300 K than at 10 K. The reason for this is that at higher temperatures there are larger numbers of atoms with sufficient energy to overcome activation energy barriers for plasticity [21]. Figure 2b shows that the variation of the average flow stress with grain size at the two different temperatures is quite similar, with similar slopes both in the Hall–Petch regime and in the inverse Hall–Petch region.

The Hall–Petch slope k for Zr, taken from hardness (HV) measurements and based on slip as the main deformation mechanism, was reported to be 0.25 MN $m^{-3/2}$ [46]. From our results $k = 3.45$ GPa $nm^{-1/2} = 0.109$ MN $m^{-3/2}$ for 300 K and $k = 3.56$ GPa $nm^{-1/2} = 0.112$ MN $m^{-3/2}$ for 10 K. Using a simple model for the relationship between hardness and flow stress $HV = 3\sigma_y$ [47], there is very good agreement between our results and experiment. Note also in Figure 2b that the experimental points at grain sizes in the micrometer regime [9] also show excellent agreement with the extrapolation of our results.

For grains smaller than a critical size we observe an inverse Hall–Petch effect (see Fig. 2b). The critical size is smaller at 300 K (20 nm) than at 10 K (30 nm). This

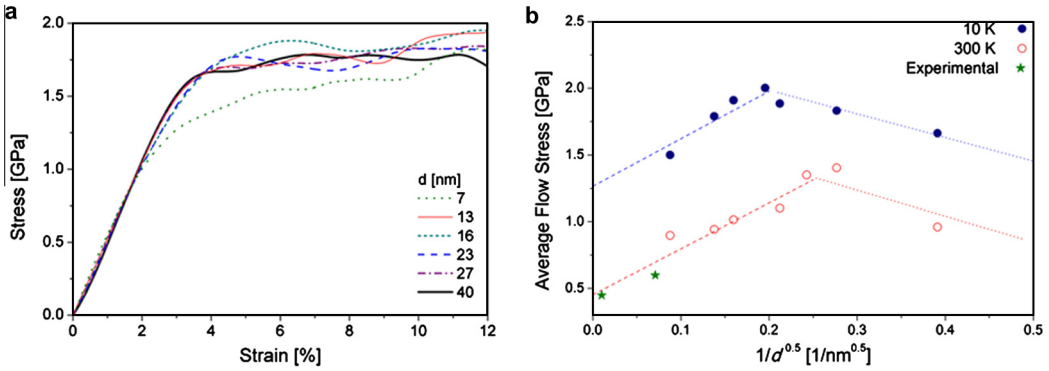

Figure 2. (a) Stress–strain curves for nc-Zr of different average grain size d at 10 K. Six-grain samples, under tension loading at a strain rate of $5 \times 10^8 s^{-1}$. (b) Average flow stresses vs. $1/d^{0.5}$ for 10 and 300 K.

is quite similar to Wang's [15] experimental results on thin films of nc-Zr with columnar grains.

The main possible mechanisms of plastic deformation in nc-Zr are emission and glide of dislocations, GB sliding and twinning. Experimentally, slip in Zr has a strong preference for the ⟨11–20⟩{1–100} first-order prismatic slip system at room temperature [27,31,32,48]. The geometry of our samples was chosen to allow the activation of the preferred slip system. We analyzed the process of dislocation emission and glide in detail.

Figure 3a shows examples of the dislocation emission process observed. The Burgers vectors, as shown in Figure 3b and c, are indeed of the ⟨11–20⟩ type and the cores are typically planar in the {1–100} plane with a width about three times the Burgers vector magnitude a, but they can be deformed if they interact with another dislocation nearby, as shown in Figure 3b and c. The core structure observed agrees well with that simulated for single dislocations [48]. Figure 3d shows the number of dislocations emitted as a function of grain size. Our results indicate that the number of dislocations involved exhibits a linear dependence on the grain size. The slopes of the linear dependence translate to approximately one dislocation for every 5.5 nm of the length of the grain boundary trace at 10 K and one dislocation every 4 nm of the length of the grain boundary trace at 300 K.

We also investigated the glide process of the emitted dislocations. The paths of individual dislocations were visualized using a grayscale plot of the displacement field, with homogenous deformations subtracted. Supplementary Fig. S1 shows the paths of dislocations observed between 6.5% and 9% strain. As seen in this visualization, the average distance traveled by the dislocations also increases with grain size. This, together with the linear dependence of the number of dislocations emitted with grain size, indicates that the contribution of dislocation activity to the total strain also increases with the grain size.

We measured the extent of grain boundary sliding as a function of grain size, using marker atoms that form a straight line crossing the grain boundary in the undeformed sample. This is shown in the insets of Supplementary Fig. S1 for the grain boundary between grains 1 and 5, which presents the most significant sliding values. The absolute magnitude of the sliding vector for this boundary increases with grain size but its contribution to deformation decreases with grain size. At 10% strain the sliding distance measured for this boundary is 12% of d (the grain size) for $d = 17$ nm and only 7% of d for $d = 131$ nm.

In this paper, we studied in detail the activated glide systems that were expected from experiments (prismatic glide along ⟨11–20⟩{1–100}) and grain boundary sliding. As a summary, we found that nc-Zr samples with columnar grains randomly oriented around [0 0 0 1] show a Hall–Petch behavior for grain sizes larger than a

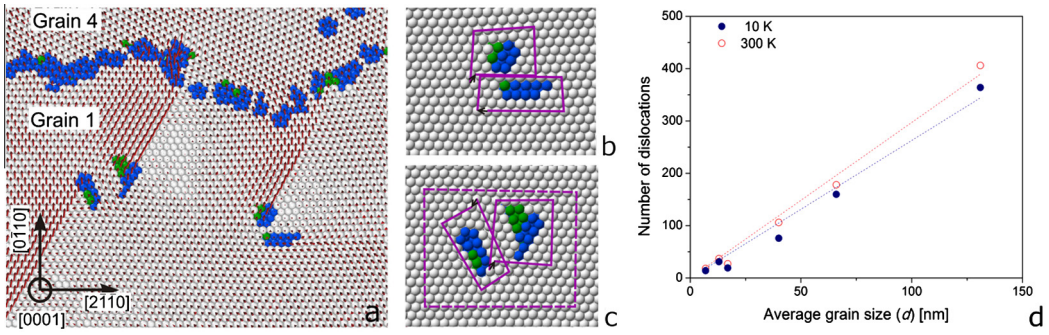

Figure 3. (a) Snapshots at 300 K, 10% strain, $d = 26$ nm, strain rate 5×10^8 s^{-1}. Atom coloring is according to CNA and red arrows indicate atomic displacements. (b and c) Burgers circuits around each dislocation are drawn in the insets. (b) Two dislocations on two different slip systems that meet. The cores are planar with a width about three times the Burgers vector magnitude, a. (c) Detail of two dislocations with opposite Burgers vector interacting. (d) Number of dislocations observed as a function of grain size and temperature in the interval between 6.5% and 9% deformation.

critical size of ~20 nm. Our results reproduced the experimental value of the Hall–Petch constant and extrapolate to experimental values for submicron grain sizes. For grains smaller than a critical size, the average flow stress of nanopolycrystalline hcp Zr decreased with decreasing grain size (inverse Hall–Petch effect). These results suggest that a grain size of the order of 10–30 nm represents the so-called "strongest size" for nanopolycrystalline hcp Zr. A detailed analysis of the deformation mechanisms shows that the number of dislocations emitted is proportional to the grain size, and increases with temperature, indicating that the number of dislocations emitted per unit length of grain boundary trace is constant with grain size. We also found that the extent of grain boundary sliding measured as a fraction of the grain size decreases with increasing grain size. The analysis suggests that GB sliding dominates plastic deformation for grains below that critical size, and dislocation emission dominates plasticity for grain sizes near and above the maximum. This interplay between dislocation-mediated deformation and grain boundary accommodation processes is qualitatively similar to observations for nanocrystalline fcc and bcc systems, despite their significantly different dislocation properties.

Support from PICT2009-0092, PIP 2011-0056, UNCuyo 06/C399 projects is greatly acknowledged. C.J.R. is grateful for financial support from an ANPCyT–UNCuyo-PRH scholarship. D.F. acknowledges support from the NSF-IRD program. The authors thank Dr. Enzo Dari for computational resources at CAB-CNEA. Helpful discussions with Dr. Carlos Tomé are acknowledged.

Supplementary data associated with this article can be found, in the online version, at http://dx.doi.org/10.1016/j.scriptamat.2013.09.010.

[1] H. Gleiter, Acta Mater. 48 (2000) 1.
[2] K.S. Kumar, H. Van Swygenhoven, S. Suresh, Acta Mater. 51 (2003) 5743.
[3] M.A. Meyers, A. Mishra, D.J. Benson, Prog. Mater. Sci. 51 (2006) 427.
[4] A.S. Argon, S. Yip, Philos. Mag. Lett. 86 (2006) 713.
[5] M. Dao, L. Lu, R.J. Asaro, J.T.M. De Hosson, E. Ma, Acta Mater. 55 (2007) 4041.
[6] J.R. Greer, J.Th.M. De Hosson, Prog. Mater. Sci. 56 (2011) 654.
[7] A. Akhtar, A. Teghtsoonian, Acta Metall. 19 (1971) 655.
[8] A.M. Garde, E. Aigeltinger, E. Reed-Hill, Metall. Trans. 4 (1973) 2461.
[9] G. Bertolino, Ph.D. Thesis, Instituto Balseiro-UNCuyo, Argentina, 2001.
[10] A.V. Podolsky, S.N. Smirnov, E.D. Tabachnikova, V.Z. Bengus, A.N. Velikodny, M.A. Tikhonovsky, et al., Low Temp. Phys. 37 (2011) 609.
[11] L. Zhang, Y. Han, J. Lu, Nanotechnology 19 (2008) 165706.
[12] C. Yuan, R. Fu, F. Zhang, X. Zhang, F. Liu, Mater. Sci. Eng. A 565 (2013) 27.
[13] D. Guo, M. Li, Y. Shi, Z. Zhang, H. Zhang, X. Liu, X. Zhang, Mater. Lett. 66 (2012) 305.
[14] M.C. Liu, J.C. Huang, H.S. Chou, Y.H. Lai, C.J. Lee, T.G. Nieh, Scripta Mater. 61 (2009) 840.
[15] Y.J. Wang, Master's thesis, National Sun Yat-sen University, Kaohsiung, Taiwan, 2010.
[16] D. Wolf, V. Yamakov, S.R. Phillpot, A. Mukherjee, H. Gleiter, Acta Mater. 53 (2005) 1.
[17] J. Schiøtz, F. Di Tolla, K.W. Jacobsen, Nature 391 (1998) 561.
[18] A. Stukowski, K. Albe, D. Farkas, Phys. Rev. B 82 (2010) 224103.
[19] D. Farkas, L. Patrick, Phil. Mag. 89 (2009) 3435.
[20] H. Van Swygenhoven, M. Spaczer, A. Caro, D. Farkas, Phys. Rev. B 60 (1999) 22.
[21] C. Brandl, P.M. Derlet, H. Van Swygenhoven, Phil. Mag. 89 (2009) 3465.
[22] A. Latapie, D. Farkas, Scripta Mater. 48 (2003) 611.
[23] H.Y. Song, Y.L. Li, J. Appl. Phys. 111 (2012) 044322.
[24] D.-H. Kim, M.V. Manuel, F. Ebrahimi, J.S. Tulenko, S.R. Phillpot, Acta Mater. 58 (2010) 6217.
[25] D.-H. Kim, F. Ebrahimi, M.V. Manuel, J.S. Tulenko, S.R. Phillpot, Mater. Sci. Eng. A 528 (2011) 5411.
[26] D-H. Kim, Ph.D. Thesis, University of Florida, 2011.
[27] E. Tenckhoff, Deformation Mechanisms, Texture and Anisotropy in Zirconium and Zircaloy, ASTM-STP-966, Philadelphia, 1988.
[28] F. Xu, R.A. Holt, M.R. Daymond, J. Nucl. Mater. 394 (2009) 9.
[29] M. Kerr, M.R. Daymond, R.A. Holt, J.D. Almer, Acta Mater. 58 (2010) 1578.
[30] S.R. Niezgoda, I.J. Beyerlein, A.K. Kanjarla, C.N. Tomé, JOM 65 (2013) 419.
[31] G.C. Kashner, C.N. Tomé, R.J. McCabe, A. Misra, S.C. Vogel, D.W. Brown, Mater. Sci. Eng. A 463 (2007) 122.
[32] L. Zhang, Y. Han, Mater. Sci. Eng. A 523 (2009) 130.
[33] J. Wang, J.P. Hirth, C.N. Tome, Acta Mater. 57 (2009) 5521.
[34] Y.T. Zhu, X.Z. Lia, X.L. Wu, Prog. Mater. Sci. 57 (2012) 1.
[35] A. Ghaderi, M. Barnett, Acta Mater. 59 (2011) 7824.
[36] I.A. Ovid'ko, N.V. Skiba, Scripta Mater. 67 (2012) 13.
[37] J. Lohmiller, R. Baumbusch, O. Kraft, P.A. Gruber, Phys. Rev. Lett. 110 (2013) 066101.
[38] S. Plimpton, J. Comput. Phys. 117 (1995) 1.
[39] R.C. Pasianot, A.M. Monti, J. Nucl. Mater. 264 (1999) 198.
[40] M.I. Mendelev, G.J. Ackland, Philos. Mag. Lett. 87 (2007) 349.
[41] E. Clouet, Phys. Rev. B 86 (2012) 144104.
[42] A. Stukowski, Modell. Simul. Mater. Sci. Eng. 18 (2010) 015012.
[43] S.G. Song, G.T. Gray III, Metall. Mater. Trans. A 26 (1995) 2665.
[44] J. Schiøtz, K.W. Jacobsen, Science 301 (2003) 1357.
[45] H.V. Swygenhoven, Science 296 (2002) 66.
[46] M.A. Meyers, O. Vohringer, V.A. Lubarda, Acta Mater. 49 (2001) 4025.
[47] M.F. Ashby, D.R.H. Jones, Engineering Materials, Butterworth-Heinemann, Oxford, 1996.
[48] H.A. Khater, D.J. Bacon, Acta Mater. 58 (2010) 2978.